

EXPERIMENTAL RESULTS ON THE AZIMUTHAL MAGNETOROTATIONAL INSTABILITY

SEILMAYER, M.¹, GALINDO, V.¹, GERBETH, G.¹, GUNDRUM, T.¹, STEFANI, F.¹, GELLERT, M.², RÜDIGER, G.², SCHULTZ, M.², HOLLERBACH, R.³

¹Helmholtz-Zentrum Dresden-Rossendorf, P.O. Box 510119, D-01314 Dresden, Germany

²Leibniz-Institut für Astrophysik Potsdam, An der Sternwarte 16, D-14482 Potsdam, Germany

³Department of Applied Mathematics, University of Leeds, Leeds LS2 9JT, UK

E-mail: M.Seilmayer@hzdr.de

Abstract: Hydrodynamically stable rotating flows can be destabilized by an azimuthal magnetic field. The arising non-axisymmetric, or azimuthal magnetorotational instability (AMRI) is important for explaining the angular momentum transport in accretion disks, and plays a central role in the concept of the MRI dynamo. We report the observation of AMRI in a magnetized liquid metal Taylor-Couette experiment, and discuss the surprisingly strong effects of a slight symmetry breaking of the applied magnetic field.

1. Introduction

Angular momentum transport in accretion disks around protostars and black holes relies on the action of the magnetorotational instability (MRI). The working principle of this instability was explained by Velikhov [1] as early as 1959. However, it took more than 30 years before Balbus and Hawley recognized its relevance for the evolution of stellar systems, X-ray binaries, and active galactic nuclei [2].

The topology of the underlying magnetic field determines the azimuthal dependence of the arising instability. While a uniform axial magnetic field threading the flow (non-zero net-flux) leads to an axisymmetric perturbation ($m = 0$), a purely azimuthal fields (zero net-flux) leads to a non-axisymmetric ($m = 1$) mode. The latter case is particularly interesting for subcritical MRI dynamos, in which the MRI-triggering field is partly sustained by the MRI-driven turbulence itself [3,4,5].

In 2005, it was shown by Hollerbach and Rüdiger [6] that the combination of an axial and an azimuthal magnetic field, giving a helical magnetic field, has a significant effect on the scaling behaviour of the MRI. This helical version of MRI (HMRI) requires only a Reynolds number $Re \sim 1000$, and a Hartmann number $Ha \sim 10$, while the standard version (SMRI), with a purely axial field being applied, requires both the magnetic Reynolds number $Rm = PmRe$ and the Lundquist number $S = Pm^{1/2}Ha$ to be in the order of 1. This grave difference in the scaling behaviour has major consequences for the effort that is needed to study the respective effects in liquid metal experiments. Actually, the HMRI has been successfully validated at the expected moderate Re and Ha numbers [7], whereas the corresponding attempts [8,9] to obtain SMRI have not yet shown conclusive results.

As for the case of a purely azimuthal field (AMRI), it was initially believed that it operates only in the same $Rm, S \gg O(1)$ parameter regime as the SMRI, and would thus be experimentally very hard to obtain [10, 11]. However, in 2010 it was discovered that for sufficiently steep rotation profiles the AMRI switches to the same inductionless (Re, Ha) parameter values as the HMRI [12]. The present paper is devoted to an experimental study of this inductionless version of the AMRI.

2. Experimental set-up

For our AMRI experiment, we utilize a slightly modified version of the PROMISE facility which has previously been used for investigations of the HMRI [7]. The main part of PROMISE is a cylindrical vessel (Fig. 1a) made of two concentric copper cylinders enclosing a cylindrical volume of height $h = 400 \text{ mm}$, and a gap width of $d = 40 \text{ mm}$ between the radii $r_{in} = 40 \text{ mm}$ and $r_{out} = 80 \text{ mm}$. This cylindrical volume is filled with the liquid eutectic alloy GaInSn whose Prandtl number is $Pm = 1.4 \times 10^{-6}$. Both the upper and lower end-caps of the cylindrical volume are formed by two plastic rings, separated at $r_{gap} = 56 \text{ mm}$, the inner and outer ring rotating with the inner and outer cylinders, respectively.

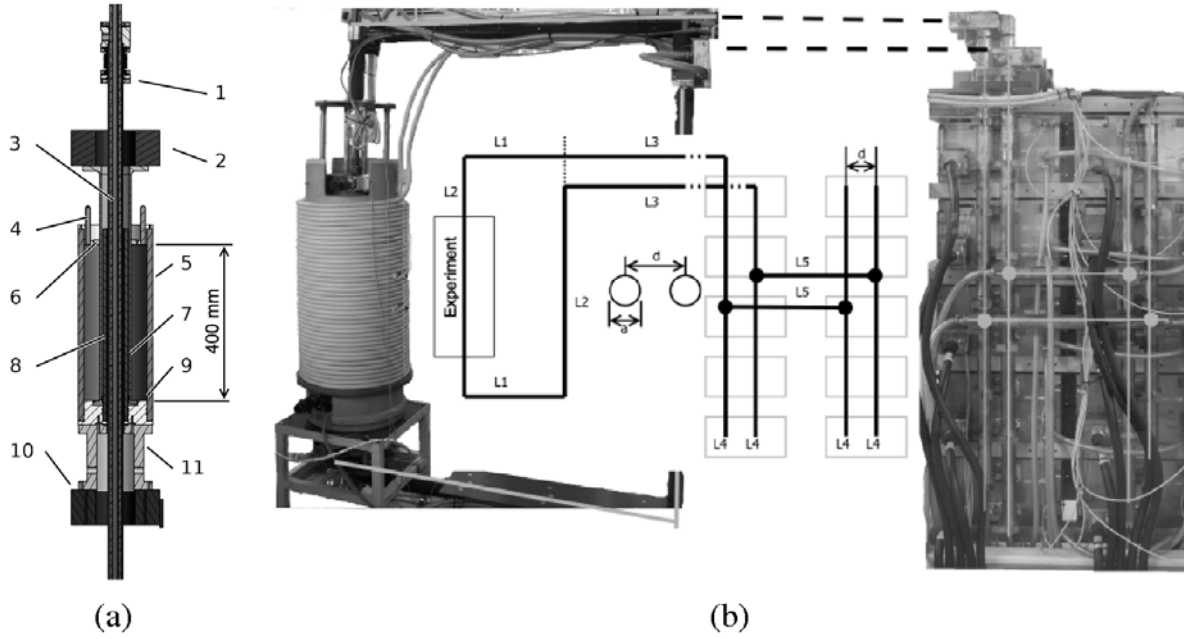


Figure 1: The present status of the PROMISE facility as used for the AMRI experiments. (a) The central Taylor-Couette module with (1) vacuum insulation for the copper rod, (2) upper motor, (3) current carrying copper rod, (4) UDV sensors, (5) outer cylinder, (6) top split rings, (7) inner cylinder, (8) center cylinder, (9) bottom split rings, (10) bottom motor, (11) spacer. (b) Modified photography of the central module, the water cooled supply rods ($a = 30 \text{ mm}$), and the power sources.

The dominantly azimuthal magnetic field is produced by a central copper rod which carries up to 20 kA . This value is approximately double the expected critical value for the onset of AMRI [12,13]. Since the central rod can become quite hot, it was thermally insulated by a vacuum tube to prevent any disturbing convection in the fluid. The rod is connected to the power source by two horizontal rods at a height of 0.8 m below the bottom and above the top of the cylindrical volume. Note that this asymmetric wiring leads to a slight deviation from a purely axisymmetric $B_\varphi(r)$, which will play an important role in the interpretation of the results. With B_z being set to zero, the AMRI is completely governed by only three non-dimensional parameters, the Reynolds number $Re := d^2 \Omega_{in} / \nu$, the ratio of outer to inner angular frequencies $\mu = \Omega_{out} / \Omega_{in}$, and the Hartmann number $Ha := B_\varphi(r_{in}) d (\sigma / \rho \nu)^{1/2}$. For converting between dimensional and non-dimensional quantities we can use the following convenient relations: $Re = 4710 \Omega_{in} / s - 1$. and $Ha = 7.77 \frac{I_{rod}}{\text{kA}}$.

For measuring the axial velocity perturbations, we use two Ultrasonic Doppler Velocimetry (UDV) transducers (from Signal Processing SA) which provide profiles of $v_z(z)$ along the beam-lines parallel to the axis of rotation. The two sensors are fixed into the outer plastic ring, **12 mm** away from the outer copper wall, and flush mounted at the interface to the GaInSn. The signals of the sensors are transferred from the rotating frame of the outer cylinder to the laboratory frame by means of a slip ring contact. Due to the strong high-frequency noise of the power supplies, numerous shielding and grounding measures were needed to improve the signal-to-noise ratio of the measurement system.

3. Results

From theoretical predictions [12,13], AMRI was expected to set in at a critical **Ha** of about **80**, which translates to a critical current of about **10 kA**. The anticipated non-axisymmetric $m = \pm 1$ spiral velocity structure, which rotates around the vertical axis with an angular frequency very close to that of the outer cylinder, can be identified by taking the difference of the signals of the two UDV transducers. In order to simulate AMRI for the real geometry of the facility and at the low **Pr** of GaInSn, we have used the OpenFoam library, enhanced by a Poisson solver for the determination of the induced electric potential (see [14] for details). The velocity structure simulated in this way can then be transformed to the co-rotating frame in order to compare the resulting velocity pattern with the experimentally observed one.

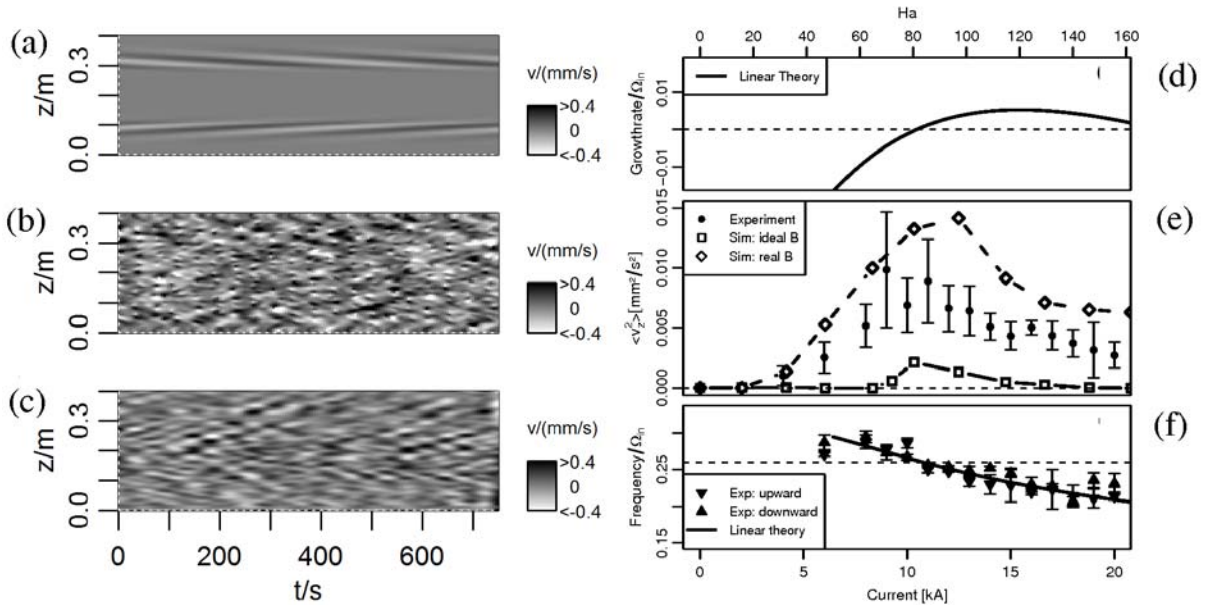


Figure 2: Results of the AMRI experiment for $\mu = 0.26$, $Re = 1480$. (a) Simulation of the velocity perturbation at $Ha = 110$ for an idealized axisymmetric field. (b) Same simulation for the realistic field. (c) Experimental results. (d) Growth rate of the AMRI as obtained from linear stability analysis, in dependence on Ha . (e) Simulated and measured mean squared velocity perturbation. (f) Angular drift frequency, with “upward” and “downward” referring to the travel direction of the velocity perturbations shown on the left side.

Figure 2a shows the result of such a simulation for the particular case $\mu = 0.26$, $Re = 1480$, $Ha = 110$, in which, as a first guess, a perfectly axisymmetric $B_\varphi(r)$ has been assumed. The resulting “butterfly” pattern represents a spiral, rotating slightly slower than the outer cylinder. Its amplitude is concentrated approximately in the middle parts of the upper and lower halves of the cylinder, where we observe a preference for either the upward moving or

the downward moving spiral. Evidently, such a symmetry breaking would not appear in an infinite length system, and must therefore be attributed to the (minor) flow modifications due to the end walls. Figure 2b shows the corresponding simulation for the case that the slight deviation of the applied magnetic field from axi-symmetry (due to the asymmetric wiring, see Figure 1b) is correctly taken into account. The effect is remarkable: the formerly clearly separated spiral structures now also fill the middle part of the cylinder and penetrate into the other halves. The corresponding velocity pattern observed in the experiment is depicted in Figure 2c and shows a great similarity with the simulation in Figure 2b. Note that a similar quasi-periodic regime of interpenetrating spirals had been observed in simulations of a co-rotating spiral Poiseuille flow [15].

A more quantitative analysis of various features of the AMRI, in dependence on Ha , is documented on the right hand side of Figure 2. Figure 2d indicates the theoretical growth rate of the AMRI as determined by a 1D-eigenvalue solver for the infinite length system [13]. In Figure 2e we show the squared rms of the UDV-measured velocity perturbation $v_z(m=1, z, t)$ and compare them with the numerically determined ones for the idealized axisymmetric field, as well as for the realistic applied magnetic field. Whereas the growth rate in Figure 2d and the numerical rms results under the axisymmetric field condition give a consistent picture, with a sharp onset of AMRI at $Ha \sim 80$, the slight symmetry breaking of the field leads, first, to some smearing out of the rms for lower Ha and, second, to a significant increase of the rms velocity value, with a reasonable correspondence of numerical and experimental values.

The dependence of the numerically and experimentally determined normalized drift frequency on Ha is given in Figure 2f. AMRI represents a $m = \pm 1$ spiral pattern that rotates approximately with the rotation rate of the outer cylinder [13]. There is still some deviation from perfect co-rotation, with a slightly enhanced frequency for lower Ha and a slightly reduced frequency for higher Ha , which can be identified both in the linear theory and in the experimental data.

4. Conclusions

We have proved that AMRI occurs in a hydrodynamically stable differential rotational flow of a liquid metal when it is exposed to a dominantly azimuthal magnetic field. The dependence of the rms and the frequency of the non-axisymmetric velocity perturbations on Ha turned out to be in good agreement with numerical predictions, especially if the simulation incorporates the slight symmetry breaking of the externally applied magnetic field. In addition to the increase of the rms value, which is mainly due to the interpenetration of the two spirals, we have observed a shift of the critical Hartmann number below the numerically predicted value of approximately 80.

Present experimental and numerical work will give an answer to the interesting question whether the AMRI shifts also to higher values of μ when the symmetry breaking of the applied field is taken into account. Actually, the general question for which steepness of the rotation profile which parameter combinations, (Re, S) or (Re, Ha) , are the relevant ones, is of astrophysical significance, since the Keplerian profile $\Omega(r) \sim r^{-3/2}$ that is of greatest interest in accretion disks is considerably shallower than the limiting Rayleigh line $\Omega(r) \sim r^{-2}$. Usually, both the HMRI as well as the AMRI switch from the (Re, Ha) scaling back to the (Re, S) scaling for rotation profiles as shallow as Keplerian, as was first noted for the HMRI by Liu et al. [16] and generalized to higher m modes by Kirillov et al. [17]. If, however, the field profiles are taken only slightly shallower than $B_\phi(r) \sim r^{-1}$, both the HMRI and the AMRI have recently been shown [18] to scale with (Re, Ha) even for Keplerian rotation profiles.

While this axisymmetric scenario would still require a significant induction effect, i.e. some $Rm \gg 1$, in the rotating fluid, a possible shift of AMRI to higher values of m for slightly non-axisymmetric, yet current-free fields could have dramatic consequences for the theory of accretion disks.

In future experiments it is also planned to investigate the influence of an additionally applied E_z , which breaks the symmetry between the $m = 1$ and $m = -1$ modes [12]. Increasing E_z even further, it should also be possible to observe the transition from the $m = \pm 1$ AMRI mode back to the previous $m = 0$ HMRI mode. A large-scale liquid sodium experiment for the combined investigation of SMRI, HMRI, AMRI, and the current-driven Tayler instability [19] is planned in the framework of the DRES-DYN project [20].

Acknowledgments.

We acknowledge financial support from Deutsche Forschungsgemeinschaft under Grant No. STE 991/1-2 and from the Helmholtz Alliance LIMTECH.

References

- [1] Velikhov, E.P.: Sov. Phys. JETP 36 (1959) 995
- [2] Balbus, S.A.; Hawley, J.F.: Astrophys. J. 376 (1991) 214
- [3] Brandenburg, A. et al.: Astrophys. J. 446 (1995) 741
- [4] Rincon, F. et al.: Phys. Rev. Lett. 98 (2007) 254502
- [5] Herault, J. et al.: Phys. Rev. E 84 (2011) 036321
- [6] Hollerbach, R.; Rüdiger, G.: Phys. Rev. Lett. 95 (2005) 124501
- [7] Stefani, F. et al.: Phys. Rev. E 80 (2009) 066303
- [8] Sisan, D.R. et al.: Phys. Rev. Lett. 93 (2004) 114502
- [9] Nornberg, M.D. et al.: Phys. Rev. Lett. 104 (2010) 074501
- [10] Ogilvie, G.I.; Pringle, J.E.: Mon. Not. R. Astr. Soc. 279 (1996) 152
- [11] Rüdiger, G. et al.: Mon. Not. R. Astr. Soc. 377 (2007) 1481
- [12] Hollerbach, R. et al.: Phys. Rev. Lett. 104 (2010) 044502
- [13] Rüdiger, G. et al.: Mon. Not. R. Astr. Soc. 438 (2014) 271
- [14] Weber, N. et al.: New J. Phys. 15 (2013) 043034
- [15] Avila, M. et al.: Phys. Fluids 18 (2006) 064101
- [16] Liu, W. et al.: Phys. Rev. E 74 (2006) 056302
- [17] Kirillov, O.N. et al.: Astrophys. J. 756 (2012) 83
- [18] Kirillov, O.N., Stefani, F.: Phys. Rev. Lett. 111 (2013) 061103
- [19] Seilmayer, M. et al.: Phys. Rev. Lett. 108 (2012) 244501
- [20] F. Stefani et al.: Magnetohydrodynamics 48 (2012) 103